Thermal-Hydraulic Analysis of the JT-60SA Central Solenoid Operation

Thermal-hydraulic analysis of the JT-60SA Central Solenoid operation

R. Bonifetto, *Associate Member, IEEE*, L. Savoldi, *Member, IEEE*, and R. Zanino, *Senior Member, IEEE*

***Abstract*—The minimum temperature margin of the JT-60SA CS coil in the standard (pulsed) operation scenario, with 5.5 MA plasma current and 75 s flattop, is computed using the state-of-the-art 4C code for different values of the coupling time constant $n\tau$. The margin is > 1 K, provided $n\tau$ < 130 ms.**

***Index Terms*—JT-60SA, superconducting magnets, temperature margin, thermal-hydraulic simulations.**

I. Introduction

IN the framework of the ITER Broader Approach, the superconducting (SC) tokamak JT-60SA, an international research and development project located at Naka, Japan, and involving Japan and Europe, is currently approaching the first plasma, which is planned before the end of 2019 [1], [2].

The JT-60SA SC magnet system [3] is composed by 18 Toroidal Field (TF) coils, the Central Solenoid (CS) and six Equilibrium Field coils. The CS is made of four modules, see Fig. 1, each composed by six octa-pancakes and one quad-pancake, wound using Nb_3Sn circle-in-square Cable-In-Conduit Conductors (CICCs), and it will operate at a peak magnetic field up to 8.9 T [3]. The 52 pancakes of each module are cooled by supercritical He (SHe) at 4.4 K, flowing in 26 cooling paths [5]. As opposed to the ITER CS case [6], the SHe inlets of each double-pancake (DP) are located at the outer radius of the magnet, see again Fig. 1. From there, the SHe flows inward following one pancake and then flows back along a neighbouring pancake, with the outlet located again at the coil outer radius [7], see Fig. 2a.

The minimum temperature margin during operation, which has to be guaranteed above 1 K [8], is assessed through a thermal-hydraulic (TH) analysis accounting for all the complex heat transfer mechanisms inside the magnet, using the 4C code [9]. 4C has been successfully validated against experimental data, see [10], [11] for two examples from the ITER Toroidal Field and Central Solenoid Model Coils, TFMC and CSMC, respectively, and also already applied to the calculation of the temperature margin (ΔT_{marg}) in the JT-60SA TF coils during normal operation [12].

In this paper, the model of the JT-60SA CS is presented and implemented in the 4C code, accounting parametrically for the thermal coupling between adjacent turns and between adjacent pancakes. The actual value of the coupling parameters used in the simulations presented here is determined based on a calibration performed against data from the JT-60SA CSMC. A series of plasma pulses in the standard scenario [13] is then simulated until periodicity is reached, including as a driver of the resulting TH transient the AC coupling losses induced by the CS current variation. The minimum temperature margin (ΔT_{marg}^{min}) during the transient is finally computed as

$$\Delta T_{marg}^{min} = \min[T_{CS}(B(x,t),\ \varepsilon,\ J_{op}(t)) - T_{strand}(x,t)] \quad (1)$$

where x is the coordinate along the CICC, B is the computed profile of the magnetic field on the conductor axis [14], ε is the strain on the Nb_3Sn filaments (conservatively assumed uniform

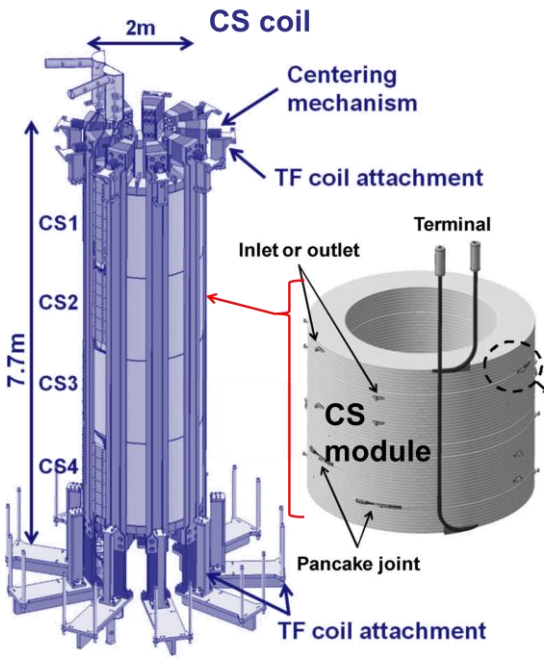

Fig. 1. Scheme of the JT-60SA CS coil and zoom on one of the 4 modules (reproduced from [4]).

Manuscript receipt and acceptance dates will be inserted here. This work has been carried out within the framework of the EUROfusion Consortium and has received funding from the Euratom research and training programme 2014-2018 under grant agreement No 633053. The work of R. Bonifetto was supported by the EUROfusion Engineering Grant. The views and opinions expressed herein do not necessarily reflect those of the European Commission. *(Corresponding author: Roberto Zanino.)*

R. Bonifetto, L. Savoldi and R. Zanino are with the NEMO Group, Dipartimento Energia, Politecnico di Torino, Torino 10129, Italy (e-mail: roberto.bonifetto@polito.it; laura.savoldi@polito.it; roberto.zanino@polito.it).

Color versions of one or more of the figures in this paper are available online at http://ieeexplore.ieee.org.

Digital Object Identifier will be inserted here upon acceptance.

and constant, equal to –0.62% from [7]), J_{op} is the operating current density and T_{strand} is the strand temperature profile computed by 4C.

As the value of the coupling time constant $n\tau$ [15] was measured on short conductor samples [8], but is affected by some uncertainty [7], a parametric study is presented to quantitatively assess the effect of $n\tau$ variation. All the input parameters and experimental data reported in this paper are based solely on publicly available literature.

II. 4C MODEL OF THE JT-60SA CS

A. Model description

The domain of the TH analysis reported in this paper is restricted to the CS2 module: the reason is that, together with its vertically symmetric module (CS3), it is the one facing the most challenging conditions in terms of peak magnetic field B (and thus heat load due to AC losses), because of its location close to the vertical center of the CS. The 4C model includes all the 26 DPs, each composed by two pancakes of 11 turns each, cooled by parallel SHe paths, and accounts for the counter-current flow in adjacent DPs, see the radial-vertical cross section of 2 DPs in Fig. 2a where the location of the He inlets and outlets is also reported. For each hydraulic channel (i.e. DP), a set of 1D Euler equations for both the hole and bundle He regions are solved along the CICC axis, coupled to each other and to the strands and jacket (for which the 1D axial heat conduction equation is solved) [16]. The geometrical data of the CS conductor and module are reported in [4]-[5], [7] and [17]-[19]. The Nb_3Sn strands adopted are identical to the ITER TF ones [2], so the same scaling used in [20] is adopted here. It results in a minimum current sharing temperature (T_{CS}) of ~ 8.6 K during operation, similar to the value measured and reported in [19].

The friction factor for the 7 mm/9 mm inner/outer diameter ITER-like spiral delimiting the central channel has been used [21], together with the Katheder friction factor recipe [22] for the bundle region: this combination showed to properly reproduce the pressure drop measurements reported in [5].

As to the thermal coupling among adjacent turns and pancakes, see Fig. 2b, the 4C code considers the turn, inter-turn (IT) and inter-pancake (IP) insulation (with a nominal thickness of 0.66 mm, 0.58 mm and 0.88 mm, respectively [4]) as a thermal resistance between two neighboring jacket sides [23], computing the equivalent heat transfer coefficient HTC_{ITIP} as:

$$HTC_{ITIP} = M \cdot k / \delta \quad (2)$$

where k is the glass-epoxy thermal conductivity, δ the total insulation thickness (see Fig. 2b) and M a fitting parameter. The latter accounts for the multi-layer nature of the insulation, introducing additional thermal contact resistances and, after the impregnation, an uncertainty on the thickness of the insulation and resin, having different thermo-physical properties.

B. Model calibration

The calibration of the IT/IP thermal coupling coefficient M is performed using experimental data from the cool-down (CD) of the JT-60SA CS Model Coil (CSMC) [7]. It consists of a CS conductor wound in a quad-pancake and DP-cooled as in the CS [5]. The available experimental data are limited to the CSMC upper DP inlet (T_{in}) and outlet (T_{out}) temperature evolution during the entire CD, and the intermediate temperature measured at the innermost turn when $T_{in}(t)$ = 100 K [7]. The CD simulation is therefore performed using as boundary conditions (BCs) the experimental T_{in} and the (unknown from literature) inlet (p_{in}) and outlet (p_{out}) pressure. While the p_{out} was set to the nominal operating value of 4.5 bar, the p_{in} was varied parametrically to best fit the measured T_{out} during the first 10 h of the CD. As also the dm/dt data are not available from literature, a mass flow rate dm/dt ~ 1.5 g/s in each DP was determined to give the best-fitting results as reported in Fig. 3; the p_{in} resulting in that mass flow rate was then kept constant during the entire CD transient. The static radiative heat load on the upper DP was

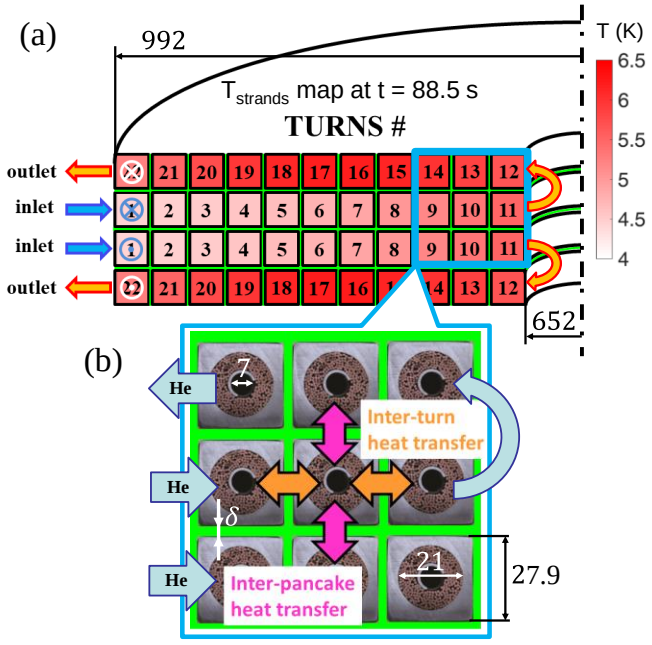

Fig. 2. 4C model of 2 CS DPs. In (a) the He inlet and outlet location is reported, showing the counter-current flow in two neighbouring cooling paths. The 2D strand temperature map computed by the 4C code in the 22 turns of the DP at t = 88.5 s is also reported. In (b) the IT/IP heat transfer paths are highlighted on a zoom of the subdomain reported in (a). The CICC cross section is reproduced from [8]. Quotes are in mm; the inner spiral diameter is quoted in (b).

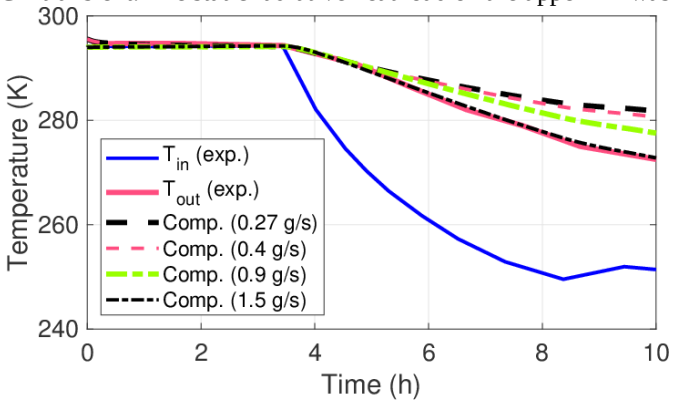

Fig. 3. Experimental (solid) and computed (dashed or dash-dotted) evolution of the T_{out} of the CSMC upper DP during the first 10 h of the CD, for different values of He dm/dt. The experimental data are taken from [7].

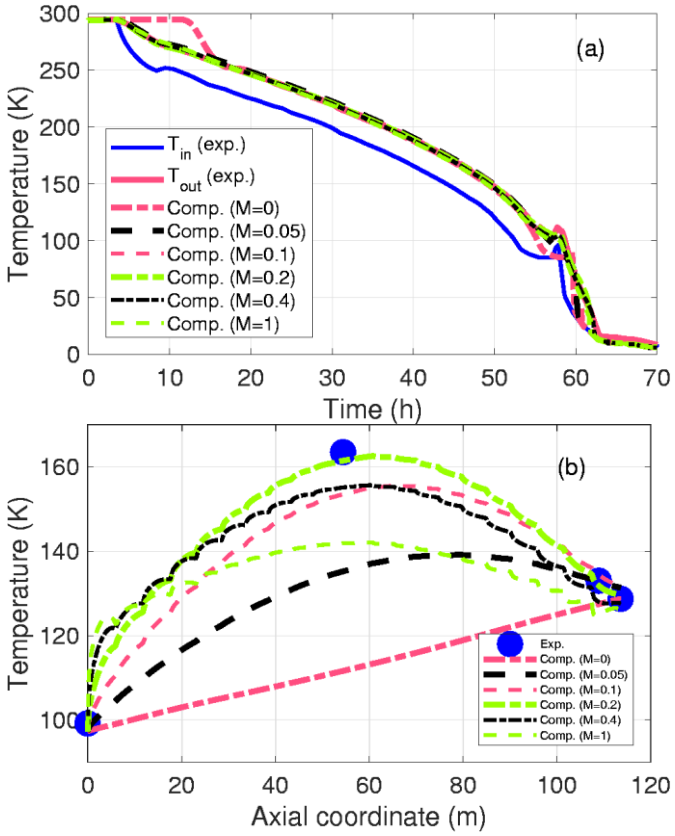

Fig. 4. (a) Experimental (solid) and computed (dashed or dash-dotted) evolution of the T_{out} of the CSMC upper DP during the CD, for different values of M. (b) Experimental (solid symbols) and computed (dashed or dash-dotted) distribution of the temperature along the upper DP of the CSMC at the time when T_{in} = 100 K (~ 53 h), for different values of M. All experimental data in this plot are taken from [7].

neglected because, as reported in [7], at least at T_{in} ~ 100 K the temperature difference between the CSMC and the thermal shield was minimized, while no information on the rest of the transient is available from literature.

The experimental T_{out} evolution is properly captured by the 4C code during the entire CD transient, see Fig. 4a. Only the adiabatic simulation (with M = 0) shows an overestimation of the outlet temperature until ~ 15 h: on one hand the cold He entering the channel reaches the solids temperature well before the outlet, while on the other hand the lack of thermal coupling between the pancakes does not allow the first turns to pre-cool the outlet turns. As a result, it takes longer for the outlet temperature to start decreasing.

After the first 15 h, Fig. 4a shows that the computed T_{out} is practically independent of M in this transient. Indeed, as the time scale of the inlet temperature decrease (~ 1000 s/K) is much longer than the He transit time in the channel (~ 30 s), the transient can be considered a sequence of quasi steady state conditions. Therefore, the outlet temperature depends only on the mass flow rate and the heat transfer coefficient between the He and the solids, which are not affected by M. The latter only modifies the heat transfer *within* the hydraulic channel, and consequently the temperature distribution along the CICC axis, see Fig. 4b.

While M decreases, the temperature peak along the channel moves towards the outlet (as expected, it is at the outlet in the adiabatic case), starting from an almost flat temperature distribution for M = 1; indeed in this case the IT/IP heat transfer time scale is much smaller than the He transit time in the hydraulic channel, so that the conduction is fast enough to homogenize the temperature on the coil radial-vertical cross section. The maximum gradient on the coil cross section, on the other hand, is reached for intermediate values of M, i.e. when the time scale of the IT/IP heat transfer is comparable with the He transit time: in this situation, the cold He flowing inwards in the first pancake of the hydraulic channel is pre-heated by the warm He flowing outwards in the second pancake, but the heat conduction is not fast enough to homogenize the temperature on the coil cross section. The best-fitting value of the HTC_{ITIP} multiplier can be determined to be 0.2, not far from the values computed e.g. in [10] and [24] for different magnets. This means that large gradients are expected to arise during the CD, so that the use of numerical tools as the 4C code is fundamental also in this slow transient to assess the maximum temperature gradient in the coil (not measurable only monitoring the inlet and outlet temperature as done, e.g., in the ITER central solenoid model coil [25]) and avoid a too fast CD possibly inducing dangerous mechanical stress in the coil, capable to damage the insulation, the jacket or the cable.

III. Simulation of the JT-60SA CS Operation

A. Simulation setup

The evolution of the CS2 operating current [13] during one plasma pulse according to the standard scenario is reported in Fig. 5a. It is used to scale the 2D magnetic field map [14] reported in Fig. 5b (computed on the conductor centerline and considered uniform on the cable cross section), corresponding to the peak current of 20 kA during the whole transient, thanks to the fact that the CS field is mostly self field. The *dB/dt* can then be evaluated and used in the single time constant formula for the determination of the AC coupling losses [26], for which $n\tau$ = 100 ms has been adopted as reference value, as it was measured on a CS conductor short sample [8]. The resulting

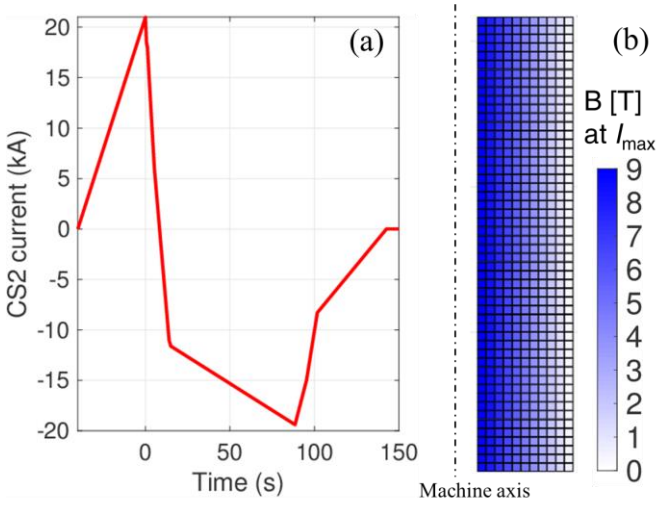

Fig. 5. (a) Evolution of the current in CS2 module during the standard scenario [13]; the duration of the entire period is 1800 s. (b) 2D distribution of the magnetic field computed when the current is at its maximum value (~ 20 kA) [14].

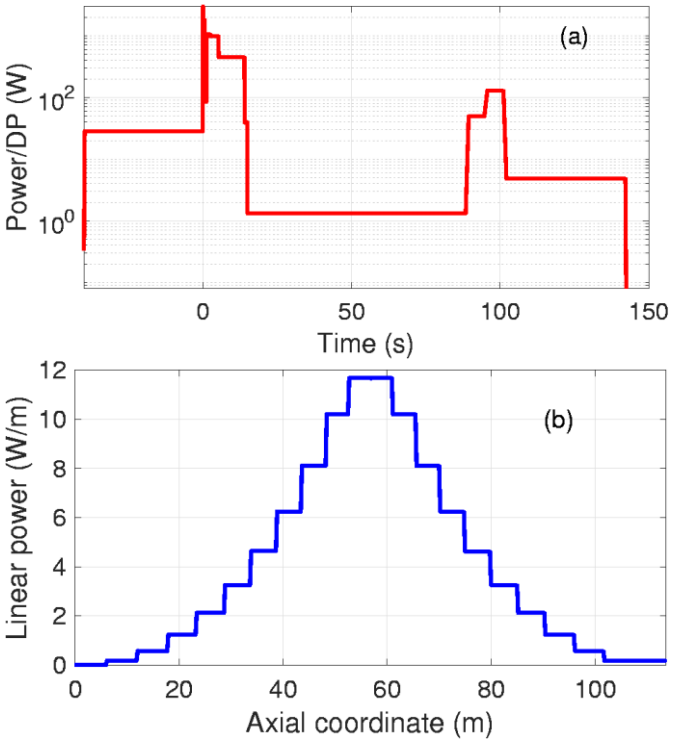

Fig. 6. (a) Evolution of the heat load on DP#10 due to AC (coupling) losses computed on the basis of the current evolution in CS2 module during the standard scenario [13]. (b) 1D distribution of the linear heat load in DP#10 between 5 and 14 s.

evolution of the heat load in the most loaded DP (#10, subject to B_{peak}) is reported in Fig. 6a. The 1D linear power distribution in the same DP is also reported for 5 s < t < 14 s in Fig. 6b, showing a peak in the central part of the hydraulic path, where the DP reaches the inner, high magnetic field side of the CS. Static and nuclear heat load are neglected in the present analysis, as they are small if compared with the AC losses [19].

The simulation is performed prescribing constant T_{in} = 4.4 K, p_{in} = 5 bar and p_{out} = 4.5 bar (resulting in the nominal mass flow rate of 6 g/s) [5].

B. Results

Periodicity of the computed results reported in this Section is achieved from the second pulse onwards.

The evolution of the strands temperature profile along DP#10, reported in Fig. 7a, shows that the initial and most intense phase of the AC losses deposition (first ~ 14 s, see Fig. 6a) is too fast to allow any escape of the heat, since advection in that region is essentially negligible (stagnation is produced in the He flow by the strong heat deposition and related pressurization, causing backflow at the inlet, see Fig. 7b, at least with the present simplistic boundary conditions) and transverse heat transfer is too ineffective (because of temperature profiles in all DPs initially all symmetric with respect to the DP center, and therefore no temperature difference to drive the heat flux). Therefore, the temperature initially evolves almost adiabatically, with the peak developing near the middle of the DP, where the heat deposition is maximum. Eventually, in the last phase of the pulse, the temperature profile starts being advected along the (by now recovered) background flow, but at the same

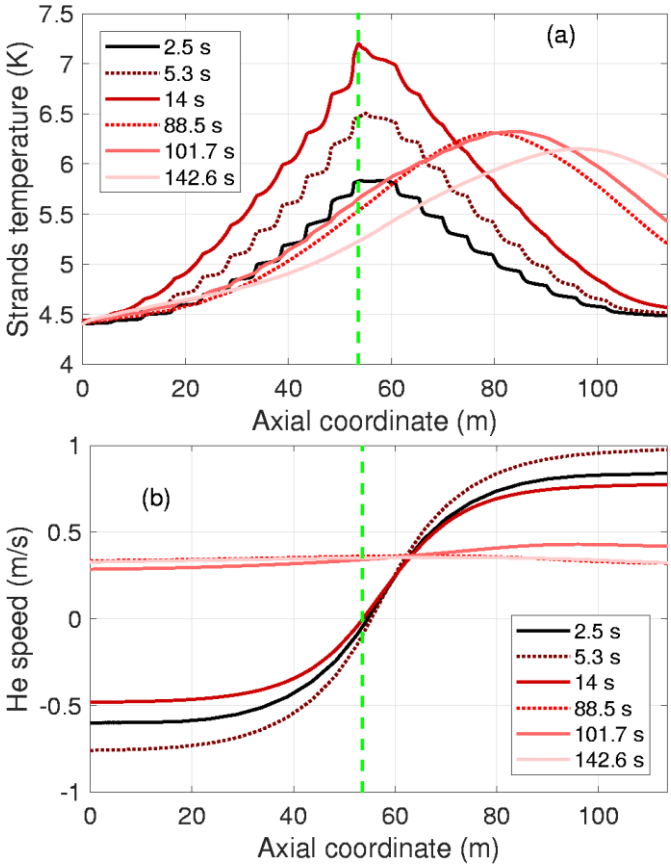

Fig. 7. Computed 1D distribution of the T_{strand} (a) and of the average He flow speed (b) along DP#10 at selected times during the periodic pulse of the standard scenario ($n\tau$ = 100 ms). The vertical dashed line identifies the location of the hot spot temperature, coincident with the He stagnation point.

time the peak decreases. This diffusive nature is obviously due to the fact that the He returning towards the coil outer radius can now cool down on the colder He in the incoming pancake of the same DP, see also the 2D strand temperature map at t = 88.5 s, reported in Fig. 2a.

The computed evolution of the hot-spot temperature is reported in Fig. 8, together with that of T_{out}. In view of the heat deposition and transfer features just discussed, the peak T_{out} turns out to be significantly (more than 1 K) smaller that the peak hot-spot temperature, confirming that the measured T_{out} cannot be used even for a rough assessment of ΔT_{marg}. Indeed,

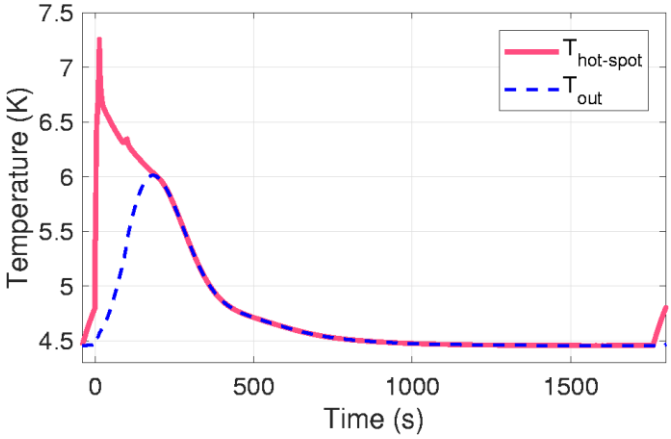

Fig. 8. Evolution of the hot-spot (solid) and outlet (dashed) temperature of DP#10 computed during the periodic pulse of the standard scenario ($n\tau$ = 100 ms).

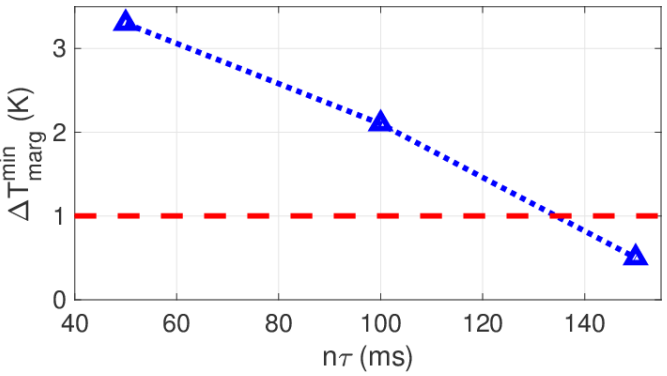

Fig. 9. Minimum temperature margin in the CS2 during the periodic pulse of the standard scenario computed for different values of the coupling time constraint ($n\tau$) of the CS conductor. The horizontal dashed line represents the minimum margin requirement for the JT-60SA CS.

ΔT_{marg} cannot be *measured*, but can only be computed by suitable TH codes, as done here.

The computed value of $\Delta T_{marg}{}^{min}$, see Eq. (1), is reported in Fig. 9 for different values of the coupling time constant, see [7] for different values identified during the CSMC tests. It is seen that, for the nominal value $n\tau = 100$ ms, $\Delta T_{marg}{}^{min} \sim 2.1$ K, which is much larger than the 1 K design limit. However, the computed $\Delta T_{marg}{}^{min}$ decreases as $n\tau$ increases and for $n\tau > \sim 130$ ms it goes below the limit, not satisfying any more the design requirement.

IV. Conclusions

The model of the JT-60SA Central Solenoid has been developed within the framework of the validated 4C thermal-hydraulic code.

The minimum temperature margin during the standard operation scenario at 5.5 MA plasma current and 75 s flattop has been estimated to be ~ 2 K, for the nominal value of the coupling time constant ~ 100 ms. However, that margin could decrease below 1 K if $n\tau$ increases above ~ 130 ms.

Using constant pressure as boundary conditions, backflow is predicted at the inlet of the CS during the initial phase of the plasma pulse, in view of the large heat deposition induced by AC losses.

Accurate and reliable, i.e. validated, thermal-hydraulic models might be instrumental in assessing possible extensions of the operational space of a tokamak plasma, without hitting onto superconducting magnet operational boundaries.

Acknowledgment

The authors thank S. Turtù for the calculation of the magnetic field map in the JT-60SA CS.

References

[1] H. Shirai, P. Barabaschi, and Y. Kamada, "Recent progress of the JT-60SA project," *Nucl. Fusion*, vol. 57, no. 10, Jun. 2017, Art. no. 102002.
[2] http://www.jt60sa.org, accessed on: Oct. 28, 2018.
[3] S. Davis, W. Abdel Maksoud, P. Barabaschi, A. Cucchiaro, P. Decool, E. Di Pietro, G. Disset, N. Hajnal, K. Kizu, C. Mayri, K. Masaki, J.-L. Marechal, H. Murakami, G. M. Polli, P. Rossi, V. Tomarchio, K. Tsuchiya, D. Tsuru, M. Verrecchia, and M. Wanner, "JT-60SA Magnet System Status," *IEEE Trans. Appl. Supercond.*, vol. 28, no. 3, Apr. 2018, Art. no. 4201707.
[4] K. Kizu, H. Murakami, K. Tsuchiya, K. Yoshida, K. Nomoto, Y. Imai, T. Minato, T. Obana, S. Hamaguchi, and K. Takahata, "Development of Central Solenoid for JT-60SA," *IEEE Trans. Appl. Supercond.*, vol. 23, no. 3, Jun. 2013, Art. no. 4200104.
[5] H. Murakami, K. Kizu, K. Tsuchiya, Y. Koide, K. Yoshida, T. Obana, K. Takahata, S. Hamaguchi, H. Chikaraishi, K. Natsume, T. Mito, S. Imagwa, K. Nomoto, and Y. Imai, "Development and Test of JT-60SA Central Solenoid Model Coil," *IEEE Trans. Appl. Supercond.*, vol. 24, no. 3, Jun. 2014, Art. no. 4200205.
[6] P. Libeyre, C. Cormany, N. Dolgetta, E. Gaxiola, C. Jong, C. Lyraud, N. Mitchell, J. Y. Journeaux, T. Vollmann, D. Evans, S. Sgobba, S. Langeslag, W. Reiersen, N. Martovetsky, D. Everitt, D. Hatfield, P. Rosenblad, S. Litherland, K. Freudenberg, L. Myatt, J. Smith, C. Brazelton, R. Abbott, J. Daubert, K. Rackers, and T. Nentwich, "Starting Manufacture of the ITER Central Solenoid," *IEEE Trans. Appl. Supercond.*, vol. 26, no. 4, Jun. 2016, Art. no. 4203305.
[7] T. Obana, H. Murakami, K Takahata, S. Hamaguchi, H. Chikaraishi, T. Mito, S. Imagawa, K. Kizu, K. Natsume, and K. Yoshida, "Performance verification tests of the JT-60SA CS model coil," *Physica C*, vol. 518, 2015, pp. 96–100.
[8] K. Nakamura, K. Nishimura, T. Masuda, T. Takao, H. Murakami, and K. Yoshida, "AC Loss and Temperature Margin of Cable-in-Conduit Conductors for JT-60SA Poloidal Field Coil," *IEEE Trans. Appl. Supercond.*, vol. 21, no. 3, Jun. 2011, pp. 2016–2019.
[9] L. Savoldi Richard, F. Casella, B. Fiori, and R. Zanino, "The 4C code for the cryogenic circuit conductor and coil modeling in ITER," *Cryogenics*, vol. 50, 2010, pp. 167–176.
[10] R. Zanino, R. Bonifetto, R. Heller, and L. Savoldi Richard, "Validation of the 4C Thermal-Hydraulic Code against 25 kA Safety Discharge in the ITER Toroidal Field Model Coil (TFMC)," *IEEE Trans. Appl. Supercond.*, vol. 21, no. 3, Jun. 2011, pp. 1948–1952.
[11] L. Savoldi, and R. Zanino, "Thermal-hydraulic analysis of T_{CS} measurement in conductor 1A of the ITER central solenoid model coil using the M&M code," *Cryogenics*, vol. 40, 2000, pp. 593–604.
[12] R. Bonifetto, P. K. Domalapally, G. M. Polli, L. Savoldi Richard, S. Turtù, R. Villari, and R. Zanino, "Computation of JT-60SA TF coil temperature margin using the 4C code," *Fus. Eng. Des.*, vol. 86, no. 6–8, Oct. 2011, pp. 1493-1496.
[13] H. Murakami, K. Kizu, K. Tsuchiya, K. Kamiya, Y. Takahashi, and K. Yoshida, "Quench detection of fast plasma events for the JT-60SA central solenoid," *Fus. Eng. Des.*, vol. 87, 2012, pp. 23–29.
[14] S. Turtù, ENEA Frascati Research Center, Via E. Fermi 45, 00044 Frascati (Italy), private communication, Jul. 2018.
[15] A. Louzguiti, L. Zani, D. Ciazynski, B. Turck, J.-L. Duchateau, A. Torre, and F. Topin, "AC Coupling Losses in CICCs: Analytical Modeling at Different Stages," *IEEE Trans. Appl. Supercond.*, vol. 27, no. 4, Jun. 2017, Art. no. 0600505.
[16] R. Zanino, S. De Palo, and L. Bottura, "A two-fluid code for the thermo-hydraulic transient analysis of CICC superconducting magnets," *J. Fusion Energy*, vol. 14, pp. 25–40, 1995.
[17] H. Urano, T. Fujita, S. Ide, Y. Miyata, G. Matsunaga, M. Matsukawa, "Development of operation scenarios for plasma breakdown and current ramp-up phases in JT-60SA tokamak," *Fus. Eng. Des.*, vol. 100, 2015, pp. 345–356.
[18] K. Nakamura, Y. Yamamoto, K. Suzuki, S. Fujiyama, T. Takao, H. Murakami, K. Natsume, and K. Yoshida, "Thermal Stability of Conductor Joint for JT-60SA Central Solenoid," *IEEE Trans. Appl. Supercond.*, vol. 26, no. 4, Jun. 2016, Art. no. 4200304.
[19] H. Murakami, K. Kizu, T. Ichige, K. Kamiya, K. Tsuchiya, K. Yoshida, T. Obana, S. Hamaguchi, K. Takahata, N. Yanagi, T. Mito, and S. Imagawa, "Current sharing temperature of central solenoid conductor for JT-60SA under repetition excitation," in *Proc. of 24th Int. Cryogenic Eng. Conf.*, Fukuoka, Japan, May 14–18, 2012, pp. 575–578.
[20] R. Zanino, R. Bonifetto, A. Brighenti, T. Isono, H. Ozeki, and L. Savoldi, "Prediction, experimental results and analysis of the ITER TF Insert Coil quench propagation tests, using the 4C code," *Supercond. Sci. Technol.*, vol. 31, 2018, Art. no. 035004.
[21] ITER Design Description Document (DDD) 11 Magnet, 2004.
[22] H. Katheder, "Optimum thermohydraulic operation regime for cable-in-conduit superconductors," *Cryogenics*, vol. 34, 1994, pp. 595–598.

[23] L. Savoldi, and R. Zanino, "M&M: multi-conductor Mithrandir code for the simulation of thermal-hydraulic transients in superconducting magnets," *Cryogenics*, vol. 40, 2000, pp. 179–189.
[24] L. Savoldi Richard, R. Bonifetto, Y. Chu, A. Kholia, S. H. Park, H. J. Lee, and R. Zanino, "4C code analysis of thermal-hydraulic transients in the KSTAR PF1 superconducting coil," *Cryogenics*, vol. 53, Jan. 2013, pp. 37–44.
[25] R. Bonifetto, A. Brighenti, T. Isono, N. Martovetsky, K. Kawano, L. Savoldi, and R. Zanino, "Analysis of the cooldown of the ITER central solenoid model coil and insert coil," *Supercond. Sci. Technol.*, vol. 30, 2017, Art. no. 015015.
[26] M. N. Wilson, *Superconducting Magnets*. Oxford, U.K.: Clarendon, 1983.